

Tractable Continuous Approximations for Constraint Selection via Cardinality Minimization

Miju Ahn^{*1}, Harsha Gangammanavar^{†1}, and David Troxell^{‡2}

¹Department of Operations Research and Engineering Management, Southern
Methodist University, Dallas TX

²Department of Statistics, Stanford University, Stanford, CA

First submission: October 14, 2022.

Abstract

We study a cardinality minimization problem that simultaneously minimizes an objective function and the cardinality of unsatisfied soft constraints. This paper proposes two continuous approximation methods which reformulate the discrete cardinality as complementarity constraints and difference-of-convex functions. We show that, under suitable conditions, local and stationary solutions of the approximation problems recover local minimizers of the cardinality minimization problem. To demonstrate effectiveness, we apply the proposed methods to applications where violating as few preference conditions (or soft constraints) is desired. The performance of the new methods is compared to benchmark formulations used in practice. Our numerical study supports the use of methods based on our new approximations for cardinality minimization that produce comparable solutions while improving computational efficiency.

1 Introduction

In this paper, we study the threshold-based cardinality minimization problems (CMP) that take the following form:

$$\min_{\mathbf{x} \in \mathcal{X}} f_0(\mathbf{x}) + \lambda \|(\max\{f_i(\mathbf{x}) - \tau_i, 0\})_{i \in [m]}\|_0. \quad (1)$$

Here, $\lambda > 0$ is the penalty parameter and $\|\bullet\|_0$ is the ℓ_0 -norm and $[m] = \{1, \dots, m\}$. The objective function $f_0(\cdot)$ and the constraints $f_i(\cdot)$ for all $i = 1, \dots, m$, are convex functions. The

*mijua@smu.edu

†harsha@smu.edu

‡dtroxell@stanford.edu

set $\mathcal{X} \subset \mathbb{R}^n$ is a compact convex set that captures what we will call the “hard constraints”. These hard constraints can be attributed to the operational requirements that cannot be violated. On the other hand, we have a set of constraints $f_i(\mathbf{x}) \leq \tau_i$ for all $i \in [m]$ that correspond to preference requirements that can be violated. The vector $\boldsymbol{\tau} = (\tau_i)_{i \in [m]}$ of these constraints captures the preference or threshold assigned by the decision maker. In this sense, the second set of constraints can be considered as “soft constraints”. While the soft constraints are allowed to be violated, the desire is to minimize the number of violations given by $\|(\max\{f_i(\mathbf{x}) - \tau_i, 0\})_{i \in [m]}\|_0$.

A form of the problem in (1) that is of particular interest to us in this paper is

$$\min_{\mathbf{x} \in \mathcal{X}} f_0(\mathbf{x}) + \lambda \|(\max\{|x_i| - \tau_i, 0\})_{i \in [n]}\|_0. \quad (2)$$

We refer to the above as the threshold-based or *two-tailed cardinality minimization problem* and denote it as τ -CMP. We obtain the τ -CMP by setting $f_i(\mathbf{x}) = |x_i|$ for all $i \in [m]$ in (1) with $m = n$. This problem essentially minimizes the count of unacceptably large elements of the vector \mathbf{x} .

It must be noted that the parameter τ_i can be absorbed into the function f_i , and we could state the soft constraints in (1) as $f_i(\mathbf{x}) \leq 0$ for all i . While the analysis we present in this paper is applicable to this modification, our choice to retain τ_i as separate parameters is to emphasize that the decision-maker can exert a choice in selecting these parameters.

A special case of (2) studied in [19] which considers the cardinality of large valued elements of \mathbf{x} exceeding the prescribed threshold $\boldsymbol{\tau}$. The authors refer to the special case as the cardinality of the upper tail minimization problem. Another notable special case of (2) is when $\tau_i = 0$ for all $i \in [n]$. The second term of (2) is often referred to as the ℓ_0 -norm, denoted $\|\mathbf{x}\|_0$, which counts the number of nonzero components of \mathbf{x} . Despite its misleading name, ℓ_0 -norm does not satisfy the properties of a norm. It is a discrete and nonconvex function, and directly minimizing a problem involving such a function is known to be computationally intractable. A predominant approach to solving such problems is by replacing the discontinuous function with the ℓ_1 -norm given by $\|\mathbf{x}\|_1 = \sum_{j=1}^n |x_j|$. This replacement results in a convex optimization problem that can be solved efficiently using off-the-shelf solvers. However, the solutions to the optimization problem with ℓ_1 -norm result in suboptimal solutions in general. This observation motivated another stream of approaches that use continuous nonconvex surrogates for the ℓ_0 -function. One such approximation related to our work is the capped- ℓ_1 function [16, 17]. This function approximates the ℓ_0 -function by the ℓ_1 -norm around the origin and a constant elsewhere. We apply a similar approximation for (2) in section 2.2.1, where we further discuss the relationship. The nonconvex approximation methods showed superior performance when applied to various applications, including image reconstruction [25], signal processing [2, 5], and deep learning methods [4].

This paper is motivated by applications where generalizing above mentioned problems involving discrete cardinality can be beneficial. Such generalization allows the optimization problem to selectively enforce soft constraints while minimizing the objective function of concern. Our

methods introduce exact and approximate reformulations of the discrete problems (1) and (2). The overarching goal of our study is to provide computationally tractable formulations and understand how one can recover solutions to the discrete problem by solving the reformulations. The problems (1) and (2) with nonzero τ arise in several application settings. The following application motivates our study.

1.1 Motivating application

Radiation therapy, specifically intensity-modulated radiation therapy (IMRT), has emerged as one of the principal treatment options for various types of cancer. IMRT is a minimally invasive treatment option where radiation of ionized beams is projected on a region of interest surrounding the tumor tissues. The region of interest includes other healthy tissues (organs at risk and normal body tissues) that are invariably exposed to radiation. Although the healthy tissues can repair themselves, limiting the exposure of organs at risk to within clinically acceptable thresholds is desirable. One achieves precise radiation delivery by shaping the dose pattern across the region of interest [13]. The desired dose pattern is generated using a multileaf collimator system by determining the angle and intensity of radiation for a set of beamlets.

We refer to the problem of designing a suitable dose pattern as the fluence map optimization problem. This problem can be formulated as a mathematical program. A clinician determines a prescription dose for the tumor and tolerance doses for organs at risk. We design the dose pattern for given values of prescription and tolerance doses. The angle and radiation amounts for the set of beamlets on the collimator constitute the decision vector of the program. The objective is to minimize the difference between radiation delivered to the tumor tissues and the prescription dose. This objective function $f_0(\cdot)$ is often modeled as a quadratic function. For an organ at risk i , the dose delivered, captured by the function $f_i(\cdot)$, must be within the tolerable dose τ_i for $i \in [m]$. With this, we see that the fluence map optimization problem takes the form of (1). We present the detailed mathematical model when we return to this problem in the numerical experiments.

While the CMP that arises in IMRT planning motivated our research, these problems are encountered in several application settings. The special case of two-tailed CMP with $\tau_i = 0 \forall i$ is prevalent in fields such as sparsity-inducing models in machine and statistical learning [8], image reconstruction [25], and signal processing [2, 5]. More general cases of CMP arise in classical combinatorial optimization problems, such as minimum irreducible infeasible subsystem cover (see, e.g., [3]), and in finance, such as portfolio selection and management [12]. An interesting application in engineering settings arises in managing transmission lines with thermal ratings in power system operations [24]. We refer the reader to the survey paper [23] for more examples of cardinality optimization problems of which CMP is a particular form.

1.2 Contribution

The main contributions of this work are threefold.

1. *Continuous approximations of the CMP.* We present two alternative continuous approximations of the CMP based on difference-of-convex (DC) programming. In the first approach, we rely upon mathematical programming with complementarity constraint (MPCC) reformulation of the CMP. This reformulation utilizes additional variables that indicate the occurrence and degree of violation, respectively. By relaxing the complementarity constraint using a penalty function that is DC-representable, we achieve a relaxed approximation of the CMP problem. We refer to this approach as the MPCC-DC. In contrast to the MPCC-DC approach, we directly develop a DC approximation of the CMP objective function in the second approach. Consequently, we refer to this approach as Direct-DC. Both our approximations are amenable to applying the difference-of-convex algorithm, thereby providing a viable solution method.
2. *Analysis of Solutions.* We develop the relationships between solutions to models that result from the alternative continuous approximations. First, we show the equivalence of the MPCC and the CMP in terms of their optimal solutions. Our subsequent analysis shows that under suitable conditions, a locally optimal solution of the MPCC-DC formulation recovers a local solution of the CMP shown in (1). For Direct-DC formulation that provides a lower bound on the CMP, we identify conditions under which we can solve the problem to global optimality. Finally, for the special case of CMP in (2), such a recovery of local optimum is achieved by a stationary solution of the Direct-DC approach. We summarize these relationships between solutions of different formulations in Figure 1.
3. *Computational validation.* We perform extensive computational experiments to compare the efficacy of our approximations. For this purpose, we utilize a CMP that arises in IMRT planning, our motivating example. In addition, we also use a portfolio optimization problem that maximizes the mean return while ensuring that the risk from investment is within tolerable limits. In the instances of the portfolio optimization problem, our approximations lead to solutions that have comparable performance to globally optimal solutions. Motivated by these results, we perform extensive experiments with the IMRT planning instances for which alternative approaches fail to provide any solution.

In addition to the numerical results presented in this paper, this work also provides analytical corroboration for our case study on a CMP problem arising in power systems planning and operations [24]. In this case study, we use the Direct-DC approach to minimize an objective function that includes counting the number of transmission lines operated outside the acceptable thermal limits.

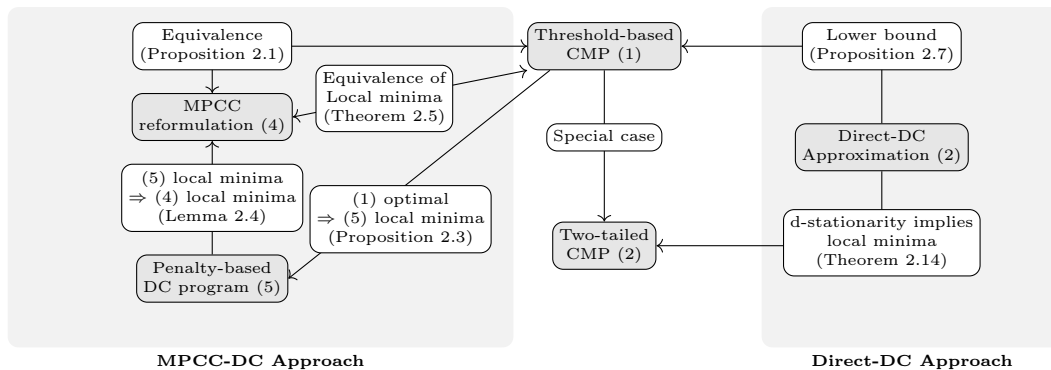


Figure 1: Schematic of the analysis in the paper showing different models and their relationships.

1.3 Notation

We define $[n] = \{1, \dots, n\}$. We use $\mathbf{x} = (x_i)_{i \in [n]}$ to denote a vector in \mathbb{R}^n where x_i is the i -th component of \mathbf{x} . Let $\mathbf{1}_n \in \mathbb{R}^n$ denote a vector of all ones. The notation $\|\mathbf{x}\|_0$ denotes the cardinality of nonzero components of \mathbf{x} . We denote an open neighborhood of radius r and center \mathbf{x} by $\mathcal{B}(\mathbf{x}, r)$.

1.4 Organization

We organize the rest of the paper as follows. In section §2, we present the two alternative continuous approximations for the CMP in (1). We also develop the relationship between the solutions of the approximate reformulations and the true problem and analyze the special case of τ -CMP in this section. In section §3, we present the results from the numerical experiments conducted on the IMRT planning problem. We summarize our conclusions in section §4.

2 Tractable Continuous Approximations

This section presents two alternative approaches to tackle the problem in (1). Both our approaches result in continuous approximations of the original problem that involve the DC program of the following form

$$\min_{\mathbf{x} \in \mathcal{X}} f(\mathbf{x}) = g(\mathbf{x}) - h(\mathbf{x}), \quad (3)$$

where \mathcal{X} is a convex closed set, and g and h are both convex. The first approach involves the DC approximation of an MPCC. On the other hand, in the second approach, we apply a DC approximation directly to the objective function of CMP.

2.1 MPCC-DC approach

In the first approach, we reformulate the ℓ_0 -function in (1) in terms of complementarity constraints. This maneuver results in an MPCC. The MPCC can, in turn, be expressed as a smooth continuous nonlinear program. In this section, we extend the reformulation approach developed in [9] to problems of the form in (1).

To obtain the so-called *full-complementarity* reformulation of (1), we introduce two auxiliary vectors $\boldsymbol{\eta} \in \mathbb{R}_+^m$ and $\boldsymbol{\xi} \in [0, 1]^m$ that are complementary to one another, that is, they satisfy the Hadamard constraint $\boldsymbol{\eta} \circ \boldsymbol{\xi} = 0$. The variable η_i takes a positive value only if $f_i(\mathbf{x}) - \tau_i > 0$ and the complementarity requirement enforces the corresponding ξ_i to zero. Consequently, a penalty of λ is incurred in the objective function. The resulting reformulation is given as

$$\begin{aligned} \min_{\mathbf{x} \in \mathcal{X}} \quad & f_0(\mathbf{x}) + \lambda \mathbf{1}_m^\top (\mathbf{1}_m - \boldsymbol{\xi}) \\ \text{subject to} \quad & \eta_i \geq f_i(\mathbf{x}) - \tau_i \quad \forall i \in [m], \\ & 0 \leq \xi_i \leq 1, \eta_i \geq 0 \quad \forall i \in [m], \\ & \boldsymbol{\eta} \circ \boldsymbol{\xi} = 0. \end{aligned} \tag{4}$$

We define a concatenated decision vector as $\mathbf{z} := (\mathbf{x}, \boldsymbol{\xi}, \boldsymbol{\eta})$ and the corresponding feasible region of the above problem without the complementarity constraint by $\mathcal{Z} := \{(\mathbf{x}, \boldsymbol{\xi}, \boldsymbol{\eta}) \mid \mathbf{x} \in \mathcal{X}, \eta_i \geq f_i(\mathbf{x}) - \tau_i, 0 \leq \xi_i \leq 1, \eta_i \geq 0, \forall i \in [m]\}$.

Based on the construction of the MPCC, it is not difficult to see that the objective function value of (4) at any feasible solution $\mathbf{z} = (\mathbf{x}, \boldsymbol{\xi}, \boldsymbol{\eta})$ upper bounds the objective function of (1) at \mathbf{x} . Furthermore, the component vector \mathbf{x}^* of the optimal solution vector $(\mathbf{x}^*, \boldsymbol{\eta}^*, \boldsymbol{\xi}^*)$ of (4) is an optimal solution to (1). We formally establish this observation regarding the equivalence of the CMP problem in (1) and the MPCC in (4) in the following proposition.

Proposition 2.1. *If \mathbf{x}^* is an optimal solution of (1) then there exists $\boldsymbol{\xi}^*$ and $\boldsymbol{\eta}^*$ such that $\mathbf{z}^* = (\mathbf{x}^*, \boldsymbol{\xi}^*, \boldsymbol{\eta}^*)$ is the optimal solution of (4). Conversely, if \mathbf{z}^* is an optimal solution of (4) then \mathbf{x}^* is an optimal solution of (1).*

Proof. To show the first statement, consider two possible cases for any given i : $f_i(\mathbf{x}^*) > \tau_i$ and $f_i(\mathbf{x}^*) \leq \tau_i$. For the former case, we must have η_i^* strictly positive, which yields $\xi_i^* = 0$ to meet the complementarity constraint of (4). For the latter, we choose $\eta_i^* = 0$ and $\xi_i^* = 1$ to achieve optimality. With the described procedure, the two problems achieve the same objective value. Since (1.1) is a lower bound for (2.2), the constructed \mathbf{z}^* is a global minimizer of (2.2). For the remaining, it suffices to show its contrapositive: if \mathbf{x}^* is not an optimal solution of (1), then \mathbf{z}^* is not optimal for (4) for any $\boldsymbol{\xi}^*$ and $\boldsymbol{\eta}^*$. Since \mathbf{x}^* is not optimal, there exists $\tilde{\mathbf{x}} \in \mathcal{X}$ such that $f_0(\mathbf{x}^*) + \lambda \|(\max\{f_i(\mathbf{x}^*) - \tau_i, 0\})_{i \in [m]}\|_0 > f_0(\tilde{\mathbf{x}}) + \lambda \|(\max\{f_i(\tilde{\mathbf{x}}) - \tau_i, 0\})_{i \in [m]}\|_0$. By applying the above argument, we can show that there does not exist \mathbf{z}^* that is optimal for (4). \square

To tackle (4), we take the approach of [14] and [15] where the problems with complementarity

constraints are reformulated as DC programs. This reformulation enables the application of the DC Algorithm [16, 22]. Specifically, we replace the complementarity constraint $\boldsymbol{\eta} \circ \boldsymbol{\xi} = 0$ in (4) by a piecewise penalty term in the objective function. This penalty term is given by

$$\rho(\boldsymbol{\eta}, \boldsymbol{\xi}) := \sum_{i=1}^m \min\{\eta_i, \xi_i\}.$$

Using the above penalty term, the full-complementarity problem in (4) can be written in the following form:

$$\min_{\mathbf{z} \in \mathcal{Z}} \{f_0(\mathbf{x}) + \lambda \mathbf{1}_m^\top (\mathbf{1}_m - \boldsymbol{\xi}) + \gamma \rho(\boldsymbol{\eta}, \boldsymbol{\xi})\}, \quad (5)$$

where $\gamma > \lambda > 0$ is another penalty parameter. By defining

$$\begin{aligned} g(\mathbf{z}) &= f_0(\mathbf{x}) + \lambda \mathbf{1}_m^\top (\mathbf{1}_m - \boldsymbol{\xi}) \text{ and} \\ h(\mathbf{z}) &= \gamma \sum_{i=1}^m \max\{-\eta_i, -\xi_i\}, \end{aligned}$$

we obtain a DC decomposition of the penalized objective function in (5). We refer to the resulting problem as MPCC-DC. It is worthwhile to note that while the objective function of (4) provides an upper bound on the CMP objective in (1), this property no longer holds when we relax the complementarity constraint in MPCC-DC. Given a feasible solution \mathbf{x} of the CMP, we can construct $(\mathbf{x}, \boldsymbol{\eta}, \boldsymbol{\xi})$ such that the MPCC-DC objective value is equal to the objective value of the CMP. However, when the solution \mathbf{x} results in a violation of $0 < f_i(\mathbf{x}) - \tau_i < \lambda/\gamma$ for some $i \in [m]$, we can construct $(\mathbf{x}, \boldsymbol{\eta}, \boldsymbol{\xi})$ such that the MPCC-DC achieves a lower objective value. We notice the significance of this interval $(0, \lambda/\gamma)$ in all the subsequent results presented in this section. To begin, the following proposition captures the nature of local solutions of (5).

Proposition 2.2. *For any local minimizer $\bar{\mathbf{z}} = (\bar{\mathbf{x}}, \bar{\boldsymbol{\xi}}, \bar{\boldsymbol{\eta}})$ of (5), we either have $0 \leq \bar{\eta}_i < \frac{\lambda}{\gamma}$ and $\bar{\xi}_i = 1$, or we have $\bar{\eta}_i \geq \frac{\lambda}{\gamma}$ and $\bar{\xi}_i = 0$ for any given i .*

Proof. For any local solution, the second and third terms in the objective of (5) are separable in i . Therefore, we can assess each soft constraint independently. There are only two cases for each component of $\rho(\bar{\boldsymbol{\eta}}, \bar{\boldsymbol{\xi}})$. For the i -th component:

$$\lambda - \lambda \bar{\xi}_i + \gamma \min\{\bar{\eta}_i, \bar{\xi}_i\} = \begin{cases} \lambda + (\gamma - \lambda) \bar{\xi}_i & \text{when } \min\{\bar{\eta}_i, \bar{\xi}_i\} = \bar{\xi}_i \\ \lambda - \lambda \bar{\xi}_i + \gamma \bar{\eta}_i & \text{when } \min\{\bar{\eta}_i, \bar{\xi}_i\} = \bar{\eta}_i. \end{cases}$$

Since $\gamma > \lambda$ and due to the local optimality of $\bar{\boldsymbol{\xi}}$, we must have $\bar{\xi}_i = 0$ and $\bar{\xi}_i = 1$ in the first

and second cases, respectively. Therefore, we can rewrite the above as

$$\lambda - \lambda\bar{\xi}_i + \gamma \min\{\bar{\eta}_i, \bar{\xi}_i\} = \begin{cases} \lambda & \text{when } \min\{\bar{\eta}_i, \bar{\xi}_i\} = \bar{\xi}_i = 0 \\ \gamma\bar{\eta}_i & \text{when } \min\{\bar{\eta}_i, \bar{\xi}_i\} = \bar{\eta}_i \leq 1 = \bar{\xi}_i. \end{cases} \quad (7)$$

Next, we show that $\bar{\eta}_i \geq \frac{\lambda}{\gamma}$ only happens with $\bar{\xi}_i = 0$. Suppose there exists some i' such that $\bar{\eta}_{i'} \geq \frac{\lambda}{\gamma}$ and $\bar{\xi}_{i'} = 1$. We can reduce the value of (7) by decreasing $\bar{\xi}_{i'}$ to 0 without affecting other components of $\bar{\mathbf{z}}$. Similarly, we can show that $0 \leq \bar{\eta}_i < \frac{\lambda}{\gamma}$ only corresponds to the case $\bar{\xi}_i = 1$. \square

The result in (7) captures the amount of penalty applied to the local minimizers of (5). Given a local minimum $\bar{\mathbf{z}}$, no penalty is applied if there is no violation of a soft constraint ($\bar{\eta}_i = 0$). When $0 < \bar{\eta}_i < \frac{\lambda}{\gamma}$, then a scaled penalty of $\gamma\bar{\eta}_i$, which is less than λ , is applied. For a larger violation magnitude $\bar{\eta}_i \geq \frac{\lambda}{\gamma}$, a penalty of λ is added, which is consistent with problems (1) and (4). Furthermore, the optimal solution of (1) and the local solution of (5) share a relationship that we identify below.

Proposition 2.3. *Let \mathbf{x}^* be an optimal solution of (1). If either $f_i(\mathbf{x}^*) - \tau_i < 0$ or $f_i(\mathbf{x}^*) - \tau_i > \frac{\lambda}{\gamma}$ for all $i \in [m]$, then there exists $(\boldsymbol{\eta}^*, \boldsymbol{\xi}^*)$ such that $(\mathbf{x}^*, \boldsymbol{\eta}^*, \boldsymbol{\xi}^*)$ is a local minimizer of (5).*

Proof. In the case of $f_i(\mathbf{x}^*) - \tau_i < 0$, choose $\eta_i^* = 0$ and $\xi_i^* = 1$. Otherwise, choose $\eta_i^* \geq f_i(\mathbf{x}^*) - \tau_i$ and $\xi_i^* = 0$. By construction and the global optimality of \mathbf{x}^* , we must have

$$\begin{aligned} f_0(\mathbf{x}^*) + \lambda \mathbf{1}_m^\top (\mathbf{1}_m - \boldsymbol{\xi}^*) + \gamma \rho(\boldsymbol{\eta}^*, \boldsymbol{\xi}^*) &= f_0(\mathbf{x}^*) + \lambda \|(\max\{f_i(\mathbf{x}^*) - \tau_i, 0\})_{i \in [m]}\|_0 \\ &\leq f_0(\mathbf{x}) + \lambda \|(\max\{f_i(\mathbf{x}) - \tau_i, 0\})_{i \in [m]}\|_0 \end{aligned}$$

for all $\mathbf{x} \in \mathcal{X}$. Now consider a sufficiently small neighborhood $\mathcal{B}(\mathbf{z}^*, r) \subseteq \mathcal{Z}$ such that $f_i(\mathbf{x}) - \tau_i < 0$ whenever $f_i(\mathbf{x}^*) - \tau_i < 0$ and $f_i(\mathbf{x}) - \tau_i > \frac{\lambda}{\gamma}$ whenever $f_i(\mathbf{x}^*) - \tau_i > \frac{\lambda}{\gamma}$. For any $\mathbf{z} \in \mathcal{B}(\mathbf{z}^*, r)$, we have

$$\lambda \|(\max\{f_i(\mathbf{x}) - \tau_i, 0\})\|_0 \leq \lambda(1 - \xi_i) + \gamma \min\{\eta_i, \xi_i\} \quad \forall i \in [m].$$

This shows that $(\mathbf{x}^*, \boldsymbol{\eta}^*, \boldsymbol{\xi}^*)$ is a local minimizer of (5). \square

While the above provides the relationship between the optimal solution of our intended target problem (1) and the local solutions of the approximate problem (5), we achieve the result only when the optimal solution satisfies additional requirements. Unfortunately, an optimal solution that does not satisfy the requirement may not correspond to any local solutions of (5). We provide an example to illustrate this fact.

Consider the following CMP with $m = n = 1$:

$$\min_{x \geq 0.75} \underbrace{4x^2}_{f_0(\mathbf{x})} + 1.75 \underbrace{\| (x^2 - 2x + 2) - 1 \|_0}_{f_1(\mathbf{x})}$$

Here, $\tau_1 = 1$ and $\lambda = 1.75$ in the above problem. Notice that the objective function reduces to

$$\begin{cases} 4x^2 + \lambda & \text{if } 0.75 < x < 1, \\ 4 & \text{if } x = 1 \text{ or } x = 0.75, \\ 4x^2 + \lambda & \text{if } x > 1. \end{cases}$$

The above implies that $x^* = 1$ and $x^* = 0.75$ are two optimal solutions to the CMP. Now consider the corresponding MPCC-DC problem with $\gamma = 2$

$$\begin{aligned} \min_{x \geq 0.75} \quad & 4x^2 + 1.75(1 - \xi_1) + 2 \min\{\eta_1, \xi_1\} \\ \text{subject to} \quad & \eta_1 \geq x^2 - 2x + 1, 0 \leq \xi_1 \leq 1. \end{aligned}$$

Notice that for $0.75 \leq x \leq 1$, we have $0 \leq f_1(x) - \tau_1 < \lambda/\gamma$. Setting $\eta_1 = f_1(x) - \tau_1$ reduces the objective function to $6x^2 - 4x + 2$. The objective function increases in $[0.75, 1]$ with a value of 2.375 at $x = 0.75$ and a value of 4 at $x^* = 1$. This establishes $x = 0.75$ as the local optimal solution of MPCC-DC. Therefore, we have an optimal solution ($x^* = 0.75$) of (1) that corresponds to a local solution to (5) and another optimal solution ($x^* = 1$) that does not have any corresponding local solutions.

Lemma 2.4. *If $\bar{\mathbf{z}} = (\bar{\mathbf{x}}, \bar{\boldsymbol{\xi}}, \bar{\boldsymbol{\eta}})$ is a local minimizer of (5) that satisfies $\bar{\eta}_i = 0$ or $\bar{\eta}_i \geq \frac{\lambda}{\gamma} \forall i \in [m]$, then it is a local minimizer of the MPCC (4).*

Proof. Since $\bar{\mathbf{z}}$ is a local minimizer, there exists $\mathcal{B}(\bar{\mathbf{z}}, r)$ such that $f_0(\bar{\mathbf{x}}) + \lambda \mathbf{1}_m^\top (\mathbf{1}_m - \bar{\boldsymbol{\xi}}) + \gamma \rho(\bar{\boldsymbol{\eta}}, \bar{\boldsymbol{\xi}}) \leq f_0(\mathbf{x}) + \lambda \mathbf{1}_m^\top (\mathbf{1}_m - \boldsymbol{\xi}) + \gamma \rho(\boldsymbol{\eta}, \boldsymbol{\xi})$ for all $\mathbf{z} \in \mathcal{B}(\bar{\mathbf{z}}, r) \cap \mathcal{Z}$. Let $\mathbf{z} = (\mathbf{x}, \boldsymbol{\xi}, \boldsymbol{\eta}) \in \mathcal{B}(\bar{\mathbf{z}}, r)$ be a solution feasible to the MPCC. Using the fact that $\boldsymbol{\eta} \circ \boldsymbol{\xi} = 0$ we have

$$\begin{aligned} f_0(\mathbf{x}) + \lambda \mathbf{1}_m^\top (\mathbf{1}_m - \boldsymbol{\xi}) &= f_0(\mathbf{x}) + \lambda \mathbf{1}_m^\top (\mathbf{1}_m - \boldsymbol{\xi}) + \gamma \sum_{i=1}^m \min\{\eta_i, \xi_i\} \\ &\geq f_0(\bar{\mathbf{x}}) + \lambda \mathbf{1}_m^\top (\mathbf{1}_m - \bar{\boldsymbol{\xi}}) + \gamma \sum_{i=1}^m \min\{\bar{\eta}_i, \bar{\xi}_i\} \\ &= f_0(\bar{\mathbf{x}}) + \lambda \mathbf{1}_m^\top (\mathbf{1}_m - \bar{\boldsymbol{\xi}}). \end{aligned}$$

The first inequality follows from the local minimizing property of $\bar{\mathbf{z}}$ with respect to the DC program (5). The last equality follows Proposition 2.2. Finally, noting that $\bar{\mathbf{z}} \in \mathcal{Z}$ and $\min\{\bar{\boldsymbol{\eta}}, \bar{\boldsymbol{\xi}}\} = 0$ implies $\bar{\boldsymbol{\eta}} \circ \bar{\boldsymbol{\xi}} = 0$, we have that $\bar{\mathbf{z}}$ is feasible to the MPCC. With this, we have completed the proof. \square

The following result establishes a means to identify a local minimum of the CMP.

Theorem 2.5. *If $\bar{\mathbf{z}}$ is a local minimum of the MPCC in (4), then $\bar{\mathbf{x}}$ is a local minimum of the CMP (1).*

Proof. Since $\bar{\mathbf{z}}$ is a local minimum of (4), there exists a sufficiently small open neighborhood $\mathcal{B}(\bar{\mathbf{z}}, r) \subseteq \mathcal{Z}$ such that (i)

$$f_0(\mathbf{x}) + \lambda \mathbf{1}_m^\top (\mathbf{1}_m - \boldsymbol{\xi}) \geq f_0(\bar{\mathbf{x}}) + \lambda \mathbf{1}_m^\top (\mathbf{1}_m - \bar{\boldsymbol{\xi}})$$

and (ii) $\eta_i \neq 0$ whenever $\bar{\eta}_i \neq 0$, for all $\mathbf{z} \in \mathcal{B}(\bar{\mathbf{z}}, r)$. Define $\mathcal{S}(\boldsymbol{\eta}) = \{i \in [m] : \eta_i \neq 0\}$. Further, consider $\mathcal{A}(\bar{\mathbf{z}}) = \{\mathbf{z} : f_0(\mathbf{x}) \geq f_0(\bar{\mathbf{x}}) - \epsilon, \forall 0 < \epsilon < \bar{\epsilon}\}$ for some $\bar{\epsilon} < \lambda$. The following two cases arise.

- Case 1: Consider $\mathbf{z} \in \mathcal{A}(\bar{\mathbf{z}}) \cap \mathcal{B}(\bar{\mathbf{z}}, r)$ such that $\mathcal{S}(\boldsymbol{\eta}) = \mathcal{S}(\bar{\boldsymbol{\eta}})$. Feasibility of $\bar{\mathbf{z}}$ to MPCC (4) implies $\bar{\boldsymbol{\eta}} \circ \bar{\boldsymbol{\xi}} = 0$. Since $\mathcal{S}(\boldsymbol{\eta}) = \mathcal{S}(\bar{\boldsymbol{\eta}})$, we have $\boldsymbol{\eta} \circ \bar{\boldsymbol{\xi}} = 0$. Therefore, $(\mathbf{x}, \boldsymbol{\eta}, \bar{\boldsymbol{\xi}}) \in \mathcal{A}(\bar{\mathbf{z}}) \cap \mathcal{B}(\bar{\mathbf{z}}, r)$ and feasible to MPCC. From the local minimum property of $\bar{\mathbf{z}}$ to MPCC, we have

$$f_0(\mathbf{x}) + \lambda \mathbf{1}_m^\top (\mathbf{1}_m - \bar{\boldsymbol{\xi}}) \geq f_0(\bar{\mathbf{x}}) + \lambda \mathbf{1}_m^\top (\mathbf{1}_m - \bar{\boldsymbol{\xi}}).$$

This implies

$$f_0(\mathbf{x}) + \lambda \|\boldsymbol{\eta}\|_0 \geq f_0(\bar{\mathbf{x}}) + \lambda \|\bar{\boldsymbol{\eta}}\|_0 \quad \forall (\mathbf{x}, \boldsymbol{\eta}, \bar{\boldsymbol{\xi}}) \in \mathcal{A}(\bar{\mathbf{z}}) \cap \mathcal{B}(\bar{\mathbf{z}}, r).$$

- Case 2: Consider $\mathbf{z} \in \mathcal{A}(\bar{\mathbf{z}}) \cap \mathcal{B}(\bar{\mathbf{z}}, r)$ such that $\mathcal{S}(\boldsymbol{\eta}) \supset \mathcal{S}(\bar{\boldsymbol{\eta}})$. For such a \mathbf{z} , we have $\|\boldsymbol{\eta}\|_0 \geq \|\bar{\boldsymbol{\eta}}\|_0 + 1$ and consequently

$$f_0(\mathbf{x}) + \lambda \|\boldsymbol{\eta}\|_0 \geq f_0(\bar{\mathbf{x}}) - \epsilon + \lambda (\|\bar{\boldsymbol{\eta}}\|_0 + 1) \geq f_0(\bar{\mathbf{x}}) + \lambda \|\bar{\boldsymbol{\eta}}\|_0 + \lambda - \epsilon \geq f_0(\bar{\mathbf{x}}) + \lambda \|\bar{\boldsymbol{\eta}}\|_0.$$

The last inequality follows from $(\lambda - \epsilon) > 0$.

□

By combining the results in Lemma 2.4 and Theorem 2.5, we have the following result.

Theorem 2.6. *If $\bar{\mathbf{z}} = (\bar{\mathbf{x}}, \bar{\boldsymbol{\xi}}, \bar{\boldsymbol{\eta}})$ is a local minimizer of (5) that satisfies $\bar{\eta}_i = 0$ or $\bar{\eta}_i \geq \frac{\lambda}{\gamma} \forall i \in [m]$, then it is a local minimizer of the CMP (1).*

2.2 Direct-DC approach

Before we discuss the Direct-DC approximation, we present the concepts of stationarity that are relevant to our purpose in this section. Consider the problem (3) where g and h are not necessarily differentiable. We first introduce the definition of a critical point.

Definition 2.1. A vector \mathbf{x}^* is a critical point of (3) if

$$0 \in \partial g(\mathbf{x}^*) - \partial h(\mathbf{x}^*) + \mathcal{N}_{\mathcal{X}}(\mathbf{x}^*)$$

where $\mathcal{N}_{\mathcal{X}}(\mathbf{x}^*)$ is the normal cone of \mathcal{X} at the point \mathbf{x}^* , i.e., $\mathcal{N}_{\mathcal{X}}(\mathbf{x}^*) = \{\mathbf{v} \in \mathbb{R}^n \mid \mathbf{v}^T(\mathbf{x} - \mathbf{x}^*) \leq 0 \ \forall \mathbf{x} \in \mathcal{X}\}$. The sets $\partial g(\mathbf{x}^*)$ and $\partial h(\mathbf{x}^*)$ are the subdifferentials of g and h at the point \mathbf{x}^* , respectively.

Another kind of stationary solution that plays a central role in our analysis is a directional stationary solution. We provide the formal definition below.

Definition 2.2. A vector \mathbf{x}^* is a d(irectional)-stationary solution of (3) if the directional derivative of $f(\mathbf{x})$ at \mathbf{x}^* is nonnegative for all feasible directions; i.e.,

$$f'(\mathbf{x}^*; \mathbf{x} - \mathbf{x}^*) \geq 0 \text{ for all } \mathbf{x} \in \mathcal{X}.$$

From the definitions, we can verify the relationship between the two types of stationary solutions. For the problem (3), d-stationarity always implies criticality but a critical point \mathbf{x}^* of (3) is a d-stationary solution only when h is differentiable at \mathbf{x}^* ; we refer to [20] for discussion of the stationary solutions.

Next, we propose an alternative approach to attain a continuous approximation of the CMP that directly uses a DC representation of the CMP objective function. For each condition $\|\max\{f_i(\mathbf{x}) - \tau_i, 0\}\|_0$ in the problem (1), we approximate the discrete term by $g_i(\mathbf{x}) - h_i(\mathbf{x})$ where g_i and h_i are defined as

$$\begin{aligned} g_i(\mathbf{x}) &= \max \left\{ \frac{1}{\varepsilon} (f_i(\mathbf{x}) - \tau_i), 0 \right\}, \\ h_i(\mathbf{x}) &= \max \left\{ \frac{1}{\varepsilon} (f_i(\mathbf{x}) - \tau_i) - 1, 0 \right\}. \end{aligned}$$

Here, $\varepsilon > 0$ is an approximation parameter. The proposed DC program is then defined as

$$\min_{\mathbf{x} \in \mathcal{X}} f_0(\mathbf{x}) + \lambda \sum_{i=1}^m [g_i(\mathbf{x}) - h_i(\mathbf{x})] \triangleq F(\mathbf{x}). \quad (9)$$

Observe that the approximation returns the same output as the discrete function when $f_i(\mathbf{x}) \leq \tau$ or $f_i(\mathbf{x}) \geq \tau + \varepsilon$. In the remaining case, the approximation returns a value between 0 and 1. This property immediately provides the following result.

Proposition 2.7. *For any $\varepsilon > 0$, the optimal objective value of the approximate DC program in (9) provides a lower bound to the optimal objective value of (1).*

Let f_0 and f_i for all $i \in [m]$ be differentiable. Furthermore, let the following assumptions hold.

(A1) There exists a scalar $\sigma \geq 0$ such that

$$f_0(\mathbf{x}) - f_0(\mathbf{y}) - \nabla f_0(\mathbf{y})^T(\mathbf{x} - \mathbf{y}) \geq \frac{\sigma}{2} \|\mathbf{x} - \mathbf{y}\|_2^2 \quad \forall \mathbf{x}, \mathbf{y} \in \mathcal{X}.$$

(A2) For each f_i , there exists $L_i \geq 0$ such that

$$0 \leq f_i(\mathbf{x}) - f_i(\mathbf{y}) - \nabla f_i(\mathbf{y})^T(\mathbf{x} - \mathbf{y}) \leq \frac{L_i}{2} \|\mathbf{x} - \mathbf{y}\|_2^2 \quad \forall \mathbf{x}, \mathbf{y} \in \mathcal{X}. \quad (10)$$

A differentiable function f satisfies the second inequality of (10) with a constant $L \geq 0$ if and only if the function $\frac{L}{2} \|\mathbf{x}\|_2^2 - f(\mathbf{x})$ is convex. This can be shown using the first-order condition of the latter function. We next show that the concave component of the DC program (9) is weakly convex under the assumption (A2). Here, we define a function f as a weakly convex function if $f(\mathbf{x}) + \rho \|\mathbf{x}\|_2^2$ is convex for some $\rho > 0$.

Lemma 2.8. *Let (A2) hold. For each $i \in [m]$, the function $\frac{\alpha_i}{2} \|\mathbf{x}\|_2^2 - h_i(\mathbf{x})$ is convex for any $\alpha_i \geq \frac{L_i}{\varepsilon}$. Moreover, the following inequality holds for each $h_i(\mathbf{x})$:*

$$h_i(\mathbf{x}) - h_i(\mathbf{y}) - h'_i(\mathbf{y}; \mathbf{x} - \mathbf{y}) \leq \frac{\alpha_i}{2} \|\mathbf{x} - \mathbf{y}\|_2^2 \quad \forall \mathbf{x}, \mathbf{y} \in \mathcal{X}.$$

Proof. For any $\mathbf{x} \in \mathcal{X}$, the function $\frac{\alpha_i}{2} \|\mathbf{x}\|_2^2 - h_i(\mathbf{x})$ has the following two cases:

$$\frac{\alpha_i}{2} \|\mathbf{x}\|_2^2 - h_i(\mathbf{x}) = \begin{cases} \frac{\alpha_i}{2} \|\mathbf{x}\|_2^2 - \frac{1}{\varepsilon} (f_i(\mathbf{x}) - \tau_i - \varepsilon) & \text{if } \frac{1}{\varepsilon} (f_i(\mathbf{x}) - \tau_i - \varepsilon) > 0; \\ \frac{\alpha_i}{2} \|\mathbf{x}\|_2^2 & \text{otherwise.} \end{cases}$$

Since each f_i satisfies (10), the function $\tilde{f}_i(\mathbf{x}) \triangleq \frac{1}{\varepsilon} (f_i(\mathbf{x}) - \tau_i - \varepsilon)$ satisfies the second inequality of (10) with the constant $\frac{L_i}{\varepsilon}$. Choosing $\alpha_i \geq \frac{L_i}{\varepsilon}$, we deduce the following from the inequality:

$$\frac{\alpha_i}{2} \|\mathbf{x}\|_2^2 - \tilde{f}_i(\mathbf{x}) \geq \frac{\alpha_i}{2} \|\mathbf{y}\|_2^2 - \tilde{f}_i(\mathbf{y}) + [\alpha_i \mathbf{y} - \nabla \tilde{f}_i(\mathbf{y})]^T(\mathbf{x} - \mathbf{y}) \quad \forall \mathbf{x}, \mathbf{y} \in \mathcal{X}.$$

This shows that $\frac{\alpha_i}{2} \|\mathbf{x}\|_2^2 - h_i(\mathbf{x})$ is convex which yields the desired inequality. \square

When f_0 is a strongly convex function, the penalty parameter λ can be carefully selected so that the corresponding d-stationary solution achieves global optimality.

Proposition 2.9. *Let (A1), with $\sigma > 0$, and (A2) hold. If λ satisfies $\sigma\varepsilon \geq \lambda \sum_{i=1}^m L_i$, then any d-stationary solution \mathbf{x}^* of (9) is also a global minimum.*

Proof. Recall that we denote the objective function of (9) as $F(\mathbf{x})$. Since $F'(\mathbf{x}^*; \mathbf{x} - \mathbf{x}^*) \geq 0$ for all $\mathbf{x} \in \mathcal{X}$, we have

$$\begin{aligned} F(\mathbf{x}) - F(\mathbf{x}^*) &\geq F(\mathbf{x}) - F(\mathbf{x}^*) - F'(\mathbf{x}^*; \mathbf{x} - \mathbf{x}^*) \\ &= f_0(\mathbf{x}) - f_0(\mathbf{x}^*) - f'_0(\mathbf{x}^*; \mathbf{x} - \mathbf{x}^*) + \\ &\quad \lambda \sum_{i=1}^m [g_i(\mathbf{x}) - g_i(\mathbf{x}^*) - g'_i(\mathbf{x}^*; \mathbf{x} - \mathbf{x}^*)] - \\ &\quad \lambda \sum_{i=1}^m [h_i(\mathbf{x}) - h_i(\mathbf{x}^*) - h'_i(\mathbf{x}^*; \mathbf{x} - \mathbf{x}^*)]. \end{aligned}$$

Using assumption (A1) for f_0 and convexity of g_i , we have

$$\begin{aligned} F(\mathbf{x}) - F(\mathbf{x}^*) &\geq \frac{\sigma}{2} \|\mathbf{x} - \mathbf{x}^*\|_2^2 - \lambda \sum_{i=1}^m [h_i(\mathbf{x}) - h_i(\mathbf{x}^*) - h'_i(\mathbf{x}^*; \mathbf{x} - \mathbf{x}^*)] \\ &\geq \frac{\sigma}{2} \|\mathbf{x} - \mathbf{x}^*\|_2^2 - \lambda \sum_{i=1}^m \frac{L_i}{2\varepsilon} \|\mathbf{x} - \mathbf{x}^*\|_2^2 \quad \forall \mathbf{x} \in \mathcal{X}, \end{aligned} \quad (11)$$

where the last inequality follows from Lemma 2.8. We complete the proof by applying the condition on the λ . \square

A result similar to Proposition 2.9 is shown in [1, Proposition 3.1]. Therein, the concave component of the DC program is defined as $\max_{i \in \mathcal{I}} h_i(\mathbf{x})$ where each h_i is a differentiable convex function. While the problem in [1] is a generalization of (9), the result in Proposition shows that a d-stationary point \mathbf{x}^* achieves global optimality over a restricted set. Although this result is well-known in the DC literature, we include it for completeness and to showcase the particular form it takes in the context of CMP.

For a general DC program shown in (3), a d-stationary solution yields a local minimum if h is a piecewise affine function. This is due to the fact that, if h is piecewise affine, there exists a neighborhood $\mathcal{B}(\mathbf{x}^*, r)$ such that $h(\mathbf{x}) - h(\mathbf{x}^*) = h'(\mathbf{x}^*; \mathbf{x} - \mathbf{x}^*)$ for all $\mathbf{x} \in \mathcal{B}(\mathbf{x}^*, r)$ [7, Section 4.2]. Applying to (11) in the proof above, we obtain the following result.

Corollary 2.10. *Let f_i be a piecewise affine convex function for all $i \in [m]$. Under (A1), a d-stationary solution \mathbf{x}^* of (9) is a local minimum.*

2.2.1 The special case of two-tailed cardinality minimization problem

The problem (2) is defined for a special case of (1) where $f_i(\mathbf{x}) = |x_i|$ for $i \in [n] = [m]$. When $\mathbf{x} \geq 0$, the term $\|(\max\{|x_i| - \tau_i, 0\})_{i=1, \dots, m}\|_0$ reduces to the cardinality upper tail introduced in [19]. Several interesting applications motivate the study of this particular cardinality condition. One example is the security-constrained economic dispatch problem in power systems we studied in [24], and another is the IMRT planning problem which we formally introduce in Section §3.

Consider vectors $\boldsymbol{\ell}, \mathbf{u} \in \mathbb{R}^n$ such that $\ell_i \leq -\tau_i$ and $\tau_i \leq u_i$ for all $i \in [n]$. Define a box constraint $\mathcal{C} \triangleq \{\mathbf{x} \mid \boldsymbol{\ell} \leq \mathbf{x} \leq \mathbf{u}\}$. For the current section, we consider a special case of (2) where (i) \mathcal{X} is a box constraint $\mathcal{X} = \mathcal{C}$, and (ii) the objective function f_0 is differentiable. Applying the DC approximation presented in (9) to the problem (2) yields the DC program

$$\min_{\mathbf{x} \in \mathcal{X}} f_0(\mathbf{x}) + \lambda \sum_{i=1}^n \left[\max \left\{ \frac{1}{\varepsilon} (|x_i| - \tau_i), 0 \right\} - \max \left\{ \frac{1}{\varepsilon} (|x_i| - \tau_i) - 1, 0 \right\} \right]. \quad (12)$$

Figure 2 illustrates one-dimensional two-tailed cardinality function $\|\max\{|x| - \tau, 0\}\|_0$ for a scalar x and the DC approximation function. When $\tau = 0$, the former is referred to as the ℓ_0 -function, and the latter reduces to the capped- ℓ_1 penalty [18]. Motivated by a recent work

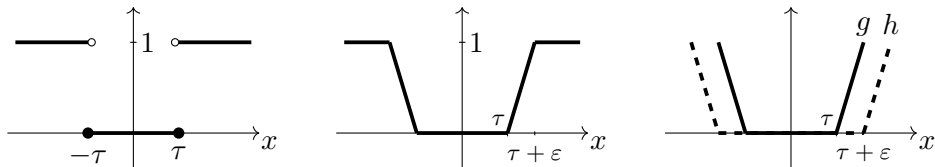


Figure 2: Let $x \in \mathbb{R}$. (Left) graph of $\|\max(|x| - \tau, 0)\|_0$; (Center) graph of the approximation function $g(x) - h(x)$ where $g(x) = \max\{\frac{1}{\epsilon}(|x| - \tau), 0\}$ and $h(x) = \max\{\frac{1}{\epsilon}(|x| - \tau) - 1, 0\}$; (Right) the DC components of the approximation: $g(x)$ is shown with solid line and $h(x)$ is shown with dashed line.

which studies the capped- ℓ_1 function for group structured sparsity problems [17], we establish the recovery of local solutions of (2) through the stationary solutions of (12). Let us assume that

(A3) There exists $\kappa \geq 0$ such that $\sup_{\mathbf{x} \in \mathcal{X}} \|\nabla f_0(\mathbf{x})\|_\infty \leq \kappa$.

Proposition 2.11. *Under Assumption (A3), let $\epsilon\kappa < \lambda$ hold. If \mathbf{x}^* is a critical point of (12) then either $|x_i^*| \leq \tau_i$ or $|x_i^*| \geq \tau_i + \epsilon$ for all $i \in [n]$.*

Proof. Suppose there exists j such that $\tau_j < |x_j^*| < \tau_j + \epsilon$. By definition of the critical point, we have

$$0 = [\nabla f_0(\mathbf{x}^*)]_j + \lambda \left(\frac{1}{\epsilon} \text{sign}(x_j^*) \right) + v_j \text{ for some } \mathbf{v} \in \mathcal{N}_{\mathcal{X}}(\mathbf{x}^*),$$

where $[\nabla f_0(\mathbf{x}^*)]_j$ is the j -th component of $\nabla f_0(\mathbf{x}^*)$. Since $\sum_{i=1}^n v_i(x_i - x_i^*) \leq 0$ for all $x_i \in [\ell_i, u_i]$ we must have $v_i = 0$ for all i . The condition $\epsilon\kappa < \lambda$ yields contradiction. \square

The above result immediately indicates that, under certain conditions, a critical point of (12) obtains the same objective value for the approximation (12) and the CMP (2). Due to the relationship between a critical point and a d-stationary solution, Proposition 2.11 also applies to any d-stationary point of (12). Before proceeding, let us define a problem for a fixed arbitrary $\bar{\mathbf{x}} \in \mathcal{X}$:

$$\begin{aligned} & \min_{\mathbf{x}} f_0(\mathbf{x}) \\ & \text{subject to } \mathbf{x} \in \widehat{\mathcal{X}}(\bar{\mathbf{x}}) \triangleq \{\mathbf{x} \in \mathcal{X} \mid |x_i| \leq \tau_i \text{ whenever } |\bar{x}_i| \leq \tau_i \forall i \in [n]\}. \end{aligned} \quad (13)$$

The above is a convex program where the constraint set is a subset of \mathcal{X} . The next two results connect the solutions of problems (12) and (2) through an optimal solution of (13).

Lemma 2.12. *Let Assumption (A3) hold. If \mathbf{x}^* is a d-stationary solution of (12) computed with $\lambda > \epsilon\kappa$, then \mathbf{x}^* is the global minimizer of (13) with feasible set $\widehat{\mathcal{X}}(\mathbf{x}^*)$.*

Proof. Denote $g_i(x_i) = \max\{\frac{1}{\varepsilon}(|x_i| - \tau_i), 0\}$ and $h_i(x_i) = \max\{\frac{1}{\varepsilon}(|x_i| - \tau_i) - 1, 0\}$. By Proposition 2.11, we either have $|x_i^*| \leq \tau_i$ or $|x_i^*| \geq \tau_i + \varepsilon$ for any i . When $|x_i^*| < \tau_i$ or $|x_i^*| > \tau_i + \varepsilon$, the derivatives of g_i and h_i are equal. The only points of interest are when $|x_i^*| = \tau_i$ and $|x_i^*| = \tau_i + \varepsilon$ where one of g_i and h_i is nondifferentiable. Therefore, by d-stationarity, \mathbf{x}^* satisfies

$$0 \leq \nabla f_0(\mathbf{x}^*)^T(\mathbf{x} - \mathbf{x}^*) + \lambda \sum_{i: |x_i^*| = \tau_i} g'_i(x_i^*; x_i - x_i^*) \\ + \lambda \sum_{i: |x_i^*| = \tau_i + \varepsilon} \left[\frac{1}{\varepsilon} \text{sign}(x_i^*)(x_i - x_i^*) - h'_i(x_i^*; x_i - x_i^*) \right] \quad \forall \mathbf{x} \in \mathcal{X}.$$

Using the fact $h'_i(x_i^*; x_i - x_i^*) = \max_{a \in \partial h_i(x_i^*)} a^T(x_i - x_i^*)$ and $\partial h_i(x_i^*) = [0, \frac{1}{\varepsilon}]$ at $x_i^* = \tau_i + \varepsilon$ and $\partial h_i(x_i^*) = [-\frac{1}{\varepsilon}, 0]$ at $x_i^* = -(\tau_i + \varepsilon)$, we verify that the last term in the above is nonpositive. Hence \mathbf{x}^* satisfies,

$$0 \leq \nabla f_0(\mathbf{x}^*)^T(\mathbf{x} - \mathbf{x}^*) + \lambda \sum_{i: |x_i^*| = \tau_i} g'_i(x_i^*; x_i - x_i^*) \\ \leq \nabla f_0(\mathbf{x}^*)^T(\mathbf{x} - \mathbf{x}^*) + \lambda \sum_{i: |x_i^*| = \tau_i} [g_i(x_i) - g_i(x_i^*)] \quad \forall \mathbf{x} \in \mathcal{X},$$

where the last inequality follows from convexity of g_i . Noting that for any i such that $|x_i^*| = \tau_i$, we have $g(x_i) = g(x_i^*) \quad \forall \mathbf{x} \in \widehat{\mathcal{X}}(\mathbf{x}^*)$ and combining with convexity of f_0 , we deduce that \mathbf{x}^* is the global minimizer of f_0 on the set $\widehat{\mathcal{X}}(\mathbf{x}^*)$. \square

The next result interprets the local minimizer of (2) in terms of the problem (13). This result is motivated by [17][Proposition 2.6].

Lemma 2.13. \mathbf{x}^* is a local minimizer of (2) if and only if \mathbf{x}^* is the global minimizer of (13) with feasible set $\widehat{\mathcal{X}}(\mathbf{x}^*)$.

Proof. Consider a sufficiently small neighborhood $\mathcal{B}(\mathbf{x}^*, \bar{r})$ centered at the local minimizer of (2), \mathbf{x}^* , such that

$$\|(\max\{|x_i^*| - \tau_i, 0\})_{i \in [n]}\|_0 = \|(\max\{|x_i| - \tau_i, 0\})_{i \in [n]}\|_0 \quad (14)$$

for all $\mathbf{x} \in \mathcal{B}(\mathbf{x}^*, \bar{r}) \cap \widehat{\mathcal{X}}(\mathbf{x}^*)$. On the other hand, by local minimality of \mathbf{x}^* , there exists $r \in (0, \bar{r}]$ such that

$$f_0(\mathbf{x}^*) + \lambda \|(\max\{|x_i^*| - \tau_i, 0\})_{i \in [n]}\|_0 \leq f_0(\mathbf{x}) + \lambda \|(\max\{|x_i^*| - \tau_i, 0\})_{i \in [n]}\|_0 \quad (15)$$

for all $\mathbf{x} \in \mathcal{B}(\mathbf{x}^*, r) \cap \mathcal{X}$. Since $\mathbf{x}^* \in \widehat{\mathcal{X}}(\mathbf{x}^*) \subseteq \mathcal{X}$, (15) applies to any $\mathbf{x} \in \mathcal{B}(\mathbf{x}^*, r) \cap \widehat{\mathcal{X}}(\mathbf{x}^*)$ which must be a nonempty set. Combining (14) and (15), we show that \mathbf{x}^* is a local minimizer of (13), which is also a global minimizer due to the convexity of the problem.

To show the other direction, consider \mathbf{x}^* which is a global minimizer of (13). For any $\mathbf{x} \in \mathcal{B}(\mathbf{x}^*, \bar{r}) \cap \widehat{\mathcal{X}}(\mathbf{x}^*)$, we have (15), achieving local minimality on the restricted set $\widehat{\mathcal{X}}(\mathbf{x}^*)$. If

\mathbf{x}^* satisfies $|x_i^*| > \tau_i$ for all i , then $\widehat{\mathcal{X}}(\mathbf{x}^*) = \mathcal{X}$ and we complete the proof. Otherwise, consider the case of $\mathcal{X} \setminus \widehat{\mathcal{X}}(\mathbf{x}^*)$; this corresponds to the case where there is at least one i such that $|x_i^*| \leq \tau_i$. There exists $r' \in (0, \bar{r})$ and $\mathcal{B}(\mathbf{x}^*, r')$ such that the following conditions hold: (i) for any $\mathbf{x} \in \mathcal{B}(\mathbf{x}^*, r')$, we have $f_0(\mathbf{x}^*) \leq f_0(\mathbf{x}) + \lambda$ due to continuity of f_0 ; and (ii)

$$\|(\max\{|x_i^*| - \tau_i, 0\})_{i \in [n]}\|_0 + 1 \leq \|(\max\{|x_i| - \tau_i, 0\})_{i \in [n]}\|_0 \quad (16)$$

for all $\mathbf{x} \in \mathcal{B}(\mathbf{x}^*, r') \cap (\mathcal{X} \setminus \widehat{\mathcal{X}}(\mathbf{x}^*))$. Hence for any $\mathbf{x} \in \mathcal{B}(\mathbf{x}^*, r') \cap (\mathcal{X} \setminus \widehat{\mathcal{X}}(\mathbf{x}^*))$, we have

$$\begin{aligned} f_0(\mathbf{x}^*) + \lambda \|(\max\{|x_i^*| - \tau_i, 0\})_{i \in [n]}\|_0 &\leq f_0(\mathbf{x}) + \lambda \left(\|(\max\{|x_i^*| - \tau_i, 0\})_{i \in [n]}\|_0 + 1 \right) \\ &\leq f_0(\mathbf{x}) + \lambda \|(\max\{|x_i| - \tau_i, 0\})_{i \in [n]}\|_0. \end{aligned}$$

This shows that \mathbf{x}^* is the local minimizer of (2). \square

Based on Lemma 2.12 and Lemma 2.13, we show that a d-stationary solution of the DC approximation problem (12) achieves local minimality of (2).

Theorem 2.14. *Let Assumption (A3) hold. If \mathbf{x}^* is a d-stationary solution of (12) computed with $\lambda > \varepsilon\kappa$, then \mathbf{x}^* is a local minimizer of (2).*

Remark 2.1. We provide two continuous approximations of CMP in (1), viz., MPCC-DC in (5) and Direct-DC in (9), that have DC expressions. We provide a relationship of local solutions between (1) and (5), utilizing the fact that we have a piecewise linear DC component. For a special case, we also show the relationship between the local solutions of (2) and d-stationary solutions of (12). The classical DC algorithm can be employed to solve the continuous approximations (as we do in our experiments reported in the next section); however, the sequence of solutions generated by this algorithm converges only to a critical point and not necessarily to a d-stationary solution. While the state-of-the-art solution methods for DC optimization, for instance, Algorithm 1 in [20], provide means to compute the d-stationary solutions for DC programs considered in this paper, they are associated with a significant computational cost. We leave the algorithmic development to address this issue as future work.

3 Computational Study

In this section, we report the results of the numerical experiments illustrating the benefits of continuous approximations. For this purpose, we use the IMRT planning problem presented in §1.1 as our motivating example and a portfolio optimization problem. To showcase the performance of the continuous approximations, we consider two alternative formulations of the CMP. These include a mixed-integer programming (MIP) model where we use a binary variable to encode when we violate a constraint. The second formulation is the extension of the MPCC in [9] that we introduced in the context of our MPCC-DC approach. For both problems, we

provide the detailed formulations in Appendix A. Unfortunately, we could not solve the MIP and MPCC model instances of the IMRT planning problem due to their large-scale nature. Therefore, we use only the portfolio optimization problem to facilitate a comparison of different modeling approaches.

3.1 Problem description

We first provide the mathematical programming formulation of the two problems and then show the numerical results.

3.1.1 Portfolio optimization problem

We consider the problem of selecting a portfolio of n assets categorized into m sectors. The objective of the optimization problem is to maximize the expected return while maintaining the sector-specific risk within tolerable limits (treated as soft constraints). We adopt the variance of returns, denoted by Σ_i for $i \in [m]$, as the risk model. The decision vector \mathbf{x} whose element, say x_j represents the percentage of total wealth we invest in asset $j \in [n]$. We model the expected return for assets as a vector $\mathbf{a} \in \mathbb{R}^n$, i.e., we expect a return of a_j if we invest the entire budget in asset $j \in [n]$. Finally, we also impose that a minimum amount, denoted by b_i , be invested in every sector $i \in [m]$. We model this problem as follows.

$$\begin{aligned} \min_{\mathbf{x}} \quad & -\mathbf{a}^\top \mathbf{x} + \lambda \sum_{i \in [m]} \|\mathbf{x}_i^\top \Sigma_i \mathbf{x}_i - \tau_i\|_0 \\ \text{subject to} \quad & \mathbf{1}_n^\top \mathbf{x} = 1, \mathbf{1}_{n_i}^\top \mathbf{x}_i \geq b_i \quad \forall i \in [m], \mathbf{x} \geq 0. \end{aligned} \tag{17}$$

In the above, we use $\mathbf{x}_i \in \mathbb{R}^{n_i}$ to denote the subvector of \mathbf{x} corresponding to assets within sector $i \in [m]$ with $\sum_{i \in [m]} n_i = n$. Using the earlier notation, we have $f_0(\mathbf{x}) = -\mathbf{a}^\top \mathbf{x}$, $f_i(\mathbf{x}) = \mathbf{x}_i^\top \Sigma_i \mathbf{x}_i$, and $\mathcal{X} = \{\mathbf{x} \mid \mathbf{1}_n^\top \mathbf{x} = 1, \mathbf{1}_{n_i}^\top \mathbf{x}_i \geq b_i \quad \forall i \in [m], \mathbf{x} \geq 0\}$.

In our numerical experiments, we use the largest "Industry Portfolios" problem instance from [10]. The data consists of $n = 49$ unique economic assets and over 5000 returns from each asset with years spanning from 1926 to 2023. We use the returns data to estimate the mean and the variance of each economic asset. We combine the 49 different assets into $m = 13$ "groups" or "sectors" of similar assets.

3.1.2 Intensity-modulated radiation therapy for cancer treatment

At the beginning of radiation therapy, a computed tomography (CT) scan provides information regarding the current state of the cancer patient. The CT scan reveals the volume of the tumor and its position in the region of interest relative to other organs at risk (OARs). The information in a CT scan is represented in terms of three-dimensional volume elements called voxels (akin to pixels in two-dimensional images). We will use $\mathcal{V} := \mathcal{T} \cup \mathcal{H}$ to denote the set of all voxels

which can be decomposed into voxels corresponding to the tumor denoted by \mathcal{T} and healthy tissues denoted by \mathcal{H} . We assume the region of interest comprises m different organ types, some of which are designated OARs. Therefore, we can obtain a further decomposition of healthy tissues as $\mathcal{H} = \cup_{i=1}^m \mathcal{H}_i$, where \mathcal{H}_i capture voxels for organ $i = 1, \dots, m$. A treatment prescription includes a target amount of radiation for the tumor and upper limits on the amount of radiation considered acceptable for all OARs. We denote the former by μ and the latter by τ_i for $i \in [m]$ (measured in unit of radiation known as Grays (Gy)).

A multileaf collimator is used to precisely conform radiation delivery to the tumor structure. Radiation is delivered by aligning the collimator beam, comprising a set of beamlets, at different gantry angles. We denote by \mathcal{B} the set of beamlets. We can control the gantry angle and the intensity of beamlets to obtain the desired dose pattern. Therefore, these constitute our primary decision variables. The amount of radiation delivered to a voxel $v \in \mathcal{V}$ is a nonlinear function of gantry angle and radiation amount. For a given gantry angle, say θ , we compute a dose deposition matrix $\mathbf{D}(\theta)$. The dose deposition matrix has a dimension of $|\mathcal{V}| \times |\mathcal{B}|$ with individual elements given by d_{vb} . We denote the intensity of a beamlet by $\mathbf{y} := (y_b)_{b \in \mathcal{B}}$. Several alternative optimization models that differ in the objective and constraints imposed are used in practice for radiation therapy planning (see [6]). For our purpose here, we consider a model that explicitly aims to achieve a precise dosage for tumor voxels while keeping the number of healthy voxels receiving more than the prescribed dosage to a minimum. We state such an optimization problem as follows:

$$\begin{aligned} \min_{\mathbf{x}, \mathbf{y}} \quad & \sum_{v \in \mathcal{T}} (x_v - \mu)^2 + \lambda \sum_{i=1}^m \left\| (\max\{|x_v| - \tau_i, 0\})_{v \in \mathcal{H}_i} \right\|_0 & (18) \\ \text{subject to } \quad & x_v = \sum_{b \in \mathcal{B}} d_{vb} y_b \quad \forall v \in \mathcal{V}, \\ & \underline{y} \leq y_b \leq \bar{y} \quad \forall b \in \mathcal{B}. \end{aligned}$$

The first set of constraints captures the amount of radiation delivered to a voxel $v \in \mathcal{V}$. The bounds on beamlet intensity are intended to capture the physical limitations of the collimator. Through the first term in the objective, the program aims to achieve precision toward tumor voxels. Mathematically, we state this term as minimizing the deviation in the amount of radiation delivered to the tumor from the prescribed dose μ . In the second term of the objective function, the individual summands represent the count of voxels of an OAR i that exceeds the prescription τ_i .

For our numerical experiments, we use the head-and-neck cancer dataset provided in [21]. The dataset includes five instances of head-and-neck cancer, each with a CT scan and a dose deposition matrix. In addition to the tumor, the CT scan of the region of interest includes four OARs (spinal cord, brainstem, left and right parotids) and unspecified normal body tissue. The prescription tumor dose is 70 Gy, and the radiation threshold for the OARs are 45, 50, and 28 Gy, respectively. Each of the five datasets has varying numbers of healthy and tumor voxels, as detailed in Table 1. We experiment with the same set of hyperparameters for all the models.

Dataset	Healthy Voxels (%)	Tumor Voxels (%)	Beamlets
1	67386 (71.0)	27576 (29.0)	3910
2	67270 (67.8)	31930 (32.2)	3888
3	76160 (67.7)	36320 (32.3)	4128
4	53176 (70.4)	22372 (29.6)	3003
5	64713 (69.3)	28638 (30.7)	3256

Table 1: Attributes for each of the five head-and-neck cancer datasets located in [21].

3.2 Experiment setup

The experiments were conducted on a computer using a 3.2 GHz 8-Core Intel processor with 32GB of RAM, running Mac OS Big Sur version 11.6. To solve the DC approximations of the CMP problem, we use the DC algorithm (DCA) [16, 22]. For completion, here we describe this algorithm using a general convex-constrained DC program, $\min_{\mathbf{x} \in \mathcal{X}} g(\mathbf{x}) - h(\mathbf{x})$:

1. Initialize $\mathbf{x}^0 \in \mathcal{X}$. Set $k = 0$.
2. Iteratively update

$$\mathbf{x}^{k+1} \in \arg \min_{\mathbf{x} \in \mathcal{X}} g(\mathbf{x}) - h(\mathbf{x}^k) - (\mathbf{v}^k)^T (\mathbf{x} - \mathbf{x}^k)$$

where $\mathbf{v}^k \in \partial h(\mathbf{x}^k)$.

3. Stop if prescribed termination criteria are satisfied.

We implemented the DCA on MATLAB and use a randomly generated initial solution vector \mathbf{x}^0 . For both the IMRT and portfolio optimization problem instances, we use Gurobi version 9.11 to solve the MIP formulations and all subproblems in the DCA. We use the MATLAB “fmincon” nonlinear optimization function for the MPCC formulation in portfolio optimization. For both the Direct-DC and MPCC-DC formulations that use the DCA, we use the relative change in solution and relative change in the objective function value as the termination criteria. Specifically, we terminate the DCA when the relative change in solution is less than 5% and the relative change in function values is less than 1%, across iterations. The “fmincon” function in MATLAB uses similar stopping criteria. For the MIP, we use the default termination criteria of Gurobi.

3.3 Numerical results

We present the numerical results for the two problems described earlier in this section.

3.3.1 Comparison of alternative approaches on portfolio optimization problem

In this section, we describe the numerical results from four alternative models of the portfolio optimization problem in (17). While the first two, a mixed-integer program and an MPCC, are exact reformulations, the last two are the continuous approximations developed in this paper. We report the mathematical formulations of these models and hyperparameters in Appendix A.1. Figures 3a and 3b show box-and-whisker plots of the mean return and number of violations, respectively.

With the MIP model, we obtain the global optimal solution. On the other hand, the solution approaches adopted for the MPCC, MPCC-DC, and Direct-DC models utilize initial solutions that we generate randomly. We replicate the experiment 30 times to get a robust sense of results that can be obtained across different initial solutions. Figure 3 displays the metrics of interest (mean return and number of violations) across all models and all trials.

In terms of mean return (see Figure 3a), the median for MPCC is more than 30% lower than the global optimal MIP solution. The median return for MPCC-DC and Direct-DC are comparable and are around 20% lower than the global optimal. In Figure 3b, we see that all four models provide comparable performance, in terms of the median number of violations, across the 30 trials. It is also noticeable that the MPCC and the MPCC-DC models are very sensitive, indicated by wider box plots for mean return and number of violations, to the choice of the initial solution. On the other hand, the Direct-DC approach shows more robust performance in our experiments. While our models only aim to minimize the number of violations, it is worthwhile to compare the magnitude of violations. Among the violated soft constraints, the MPCC method has the highest average violation magnitude, while the MPCC-DC method has the lowest violation magnitude on average. Most noticeably, the MPCC method results in a risk for $i = 13$ that is 2000% higher, on average, than the tolerable limit.

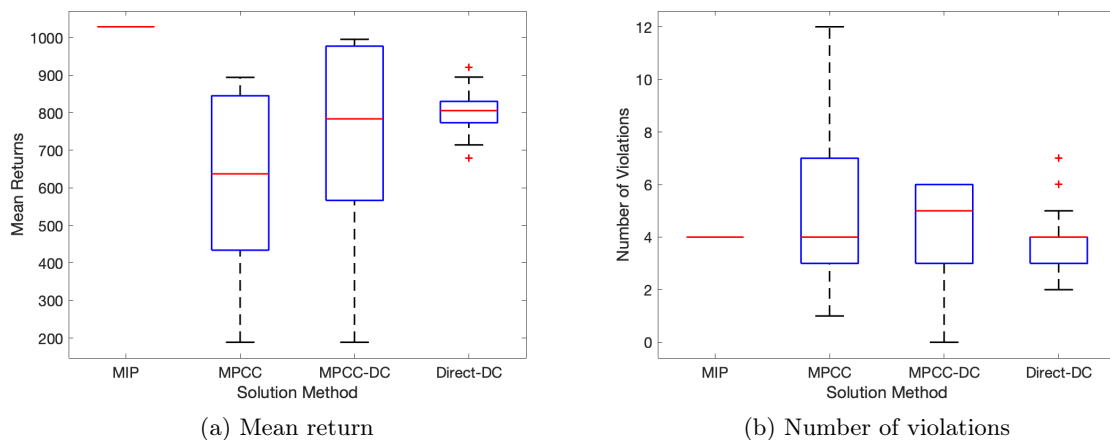


Figure 3: Results for all four portfolio optimization problem models.

3.3.2 IMRT: Performance of Direct-DC and MPCC-DC approaches

In our previous experiment, we see that the Direct-DC and MPCC-DC continuous approximation approaches provide comparable solutions to some non-continuous methods. Therefore, we employ both approaches for our experiments with the large-scale problem of IMRT planning. We investigate the performance of our continuous approximation models relative to the quadratic programming-based benchmark formulations prevalent in radiation therapy planning. The detailed formulation of these benchmarks, as well as the Direct-DC and MPCC-DC approximations, are provided in Appendix A.2.

We evaluate the performance in terms of the dosage received by tumorous and healthy voxels. Two primary questions guide this investigation.

- How many healthy voxels receive an amount of radiation exceeding their prescribed threshold, and what are the magnitudes of these violations?
- How many tumorous voxels do not receive as much radiation as prescribed, and how closely do these dosage patterns align with the prescribed amount?

Since the primary goal of IMRT is to keep healthy voxels free of exposure while administering sufficient radiation to tumorous voxels, we gain a complete view of each model’s efficacy by investigating these two questions.

The only input parameter for the Direct-DC approach is the value of ε , so we begin by studying the effect of ε on the radiation pattern. We chose $\varepsilon = \{10^{-6}, 10^{-4}, 0.01, 1, 10\}$ for this experiment. For each value, we use the decision vector obtained when the DCA is terminated to compute the dosage received by the OAR and voxels. We present these results in the dose-volume histogram in Figure 4. A dose-volume histogram depicts the percentage of voxels that receive at least as much radiation as shown in the horizontal axis. In Figure 4a, we clearly see that with smaller ε values, we ensure no healthy voxels in the left parotid organ receive radiation beyond its prescribed threshold of 28 Gy. Conversely, however, we see in the rightward plot that the solutions with the same ε values deviate more from the prescribed threshold for tumorous voxels. This trade-off between healthy and tumor voxel radiation amounts persists for larger ε values. When $\varepsilon \geq 1$, the program ensures tumorous voxels receive radiation dosages very close to the prescribed threshold of 70, yet many healthy voxels receive excess radiation. A similar observation was made in other OARs and datasets. For the remainder of experiments with the Direct-DC approach, we use $\varepsilon = 1$ as it demonstrated a reasonable compromise between radiation precision for tumors and overdosing of the healthy tissues.

In the MPCC-DC model, we observe the same trade-off between adherence to radiation prescriptions for tumorous voxels and the resistance to expose OARs to excess radiation. We choose a hyperparameter grid of $\lambda = \{.01, .1, 1, 10, 100\}$ and $\gamma = \{.5, 1, 10, 50, 250\}$, only testing combinations where $\gamma > \lambda$ (as assumed in the model). Based on our experiments, we use $\lambda = .01$ and $\gamma = 10$ that provide a degree of compromise comparable to that observed with the Direct-DC

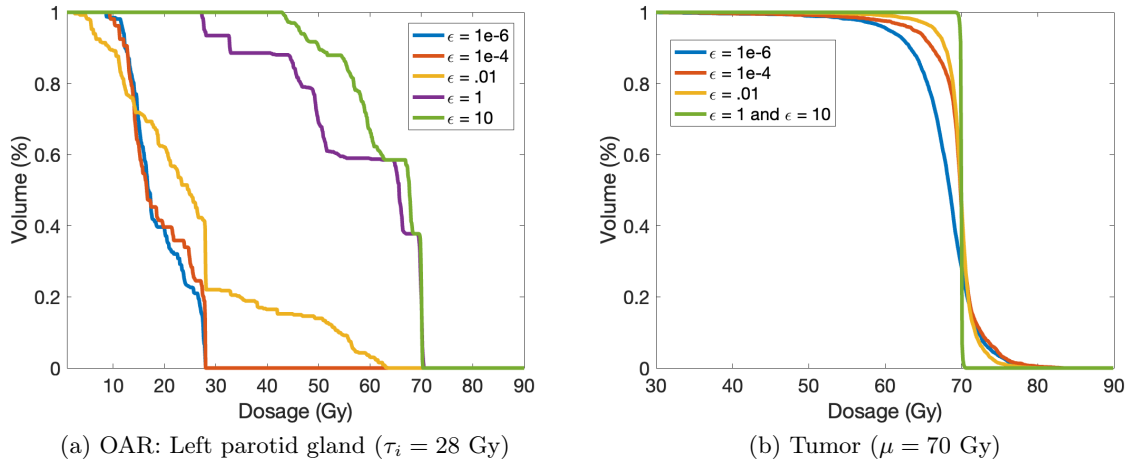
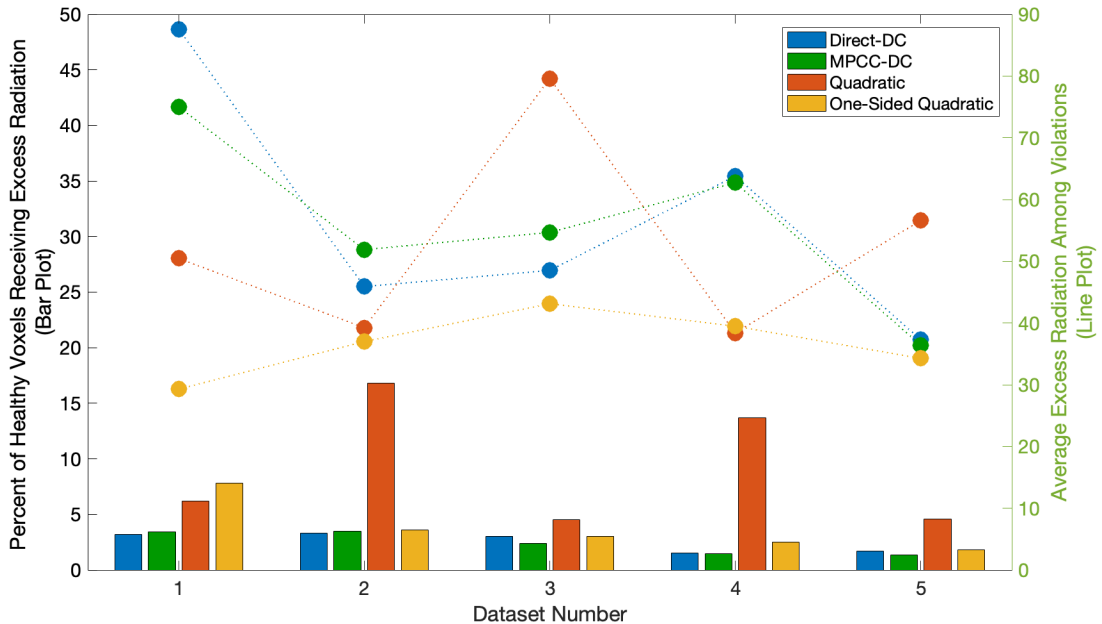
Figure 4: Dosage volume histograms for varying ϵ in the Direct-DC method for Dataset 1.

Figure 5: Percent of total healthy voxels receiving excess radiation (bar plot) and corresponding average violation magnitude as a percentage above the prescribed threshold (line plot).

approach. We note that the MIP and MPCC methods failed to converge to any solutions within the user-defined time limit of one hour. Therefore, we use quadratic-penalty (QP) and one-sided quadratic-penalty (1-QP) models as viable benchmarks for comparison. These models are well-accepted in the radiation therapy literature (see [11]) and are also presented in Appendix A.2. Based on hyperparameter selection procedures, we identified $\alpha = 1 - 10^{-6}$ for QP and $\bar{\lambda} = 0.01$ for the 1-QP.

First, we investigate the number of healthy voxel violations and the degree of these violations for all three methods. We summarize these results in Figure 5. While the percent total of healthy voxels that receive excess radiation is less than 3.5% for all datasets for the Direct-DC and

MPCC-DC methods, it reaches as high as 16.8% for the QP. Furthermore, the Direct-DC and MPCC-DC methods have equal or lesser percentages of healthy voxels receiving excess radiation than both non-DC benchmark methods in all 5 datasets. In addition to the number of healthy violations, we can also view the severity of each violation.

For each method, the line plot in Figure 5 shows the average amount of violations as a percentage of their respective prescribed threshold (computed across all the OAR). The figure shows that the average magnitude of violations is greater for the DC when compared to 1-QP for all five datasets. This behavior is expected as the penalty term for the DC methods penalizes the number while the 1-QP penalizes the degree of violations. The QP model, on the other hand, equally penalizes deviation on both sides of the prescribed dosage. Therefore, we do not notice any specific pattern in terms of overdosing the healthy voxels. Our results show that in many cases where healthy voxels receive excess radiation, the radiation amount is 0% – 5% above the prescribed threshold. For some healthy voxels, we observe radiation levels as high as 150% greater than the prescribed threshold. However, excessive overdosing is far less ubiquitous in the DC and 1-QP methods than the the QP method. Therefore, we see that not only do the DC methods consistently lead to fewer healthy voxels over-radiation, but they drastically reduce occurrences of severe burning as well. IMRT not only aims to protect healthy tissue, but it also must apply the correct amount of radiation to tumor cells. We also investigate the performance of our models on radiation to tumor voxels to answer our second question. Since all four models use the quadratic penalty to enforce precision for tumor tissue, we notice that about 50% of the tumor voxels are underdosed. Furthermore, the amount by which these tumor voxels are underdosed is also comparable across the methods.

Overall, a clear trade-off exists between adherence to dose prescriptions for healthy tumorous voxels as hyperparameter values change for the Direct-DC and MPCC-DC methods. These methods result in fewer healthy voxels that receive excess radiation beyond the prescribed threshold. While the Direct-DC and MPCC-DC violations are typically more severe on average, the number of severely overdosed voxels are fewer when compared to the QP method. Furthermore, all three methods perform similarly in regards to radiation precision to tumor voxels. Noting too that the MIP formulation failed to provide a solution to any dataset within the set timeframe, our experiments suggest that the Direct-DC and MPCC-DC methods are effective approaches for IMRT planning problems involving cardinality minimization.

4 Conclusions

In this paper, we study an optimization problem that emphasizes on minimizing the cardinality of unsatisfied constraints. The problem is motivated by an application that aims to deliver as many soft constraints in addition to minimizing the objective function subject to hard constraints. To provide computationally viable solution methods, we introduce continuous reformulations that approximate the discrete cardinality. Our analysis shows that local solutions of the cardinality minimization problem are obtainable by computing local and stationary solutions of the

proposed reformulations. We study the effectiveness of the new methods by comparing their computational performance to alternative formulations. The numerical results indicate that the proposed methods produce comparable solutions. Specifically, our study on the IMRT dataset demonstrates that our methods are capable of computing solutions with a minimal number of unsatisfied soft conditions as desired.

Acknowledgments

We thank the Associate Editor for handling our submission. We thank the two anonymous referees whose thorough review and insightful comments greatly improved the content of this paper.

A Benchmark and Approximate Formulations

In this section, we present all the formulations of the two problems used in our numerical experiments.

A.1 Portfolio optimization problem

To benchmark the developed continuous approximation, we use the MPCC and MIP formulations of the portfolio optimization problem in §3.1.1. The MIP formulation is given as

$$\begin{aligned} \min_{\mathbf{x}} \quad & -\mathbf{a}^\top \mathbf{x} + \lambda \sum_{i \in [m]} z_i \\ \text{subject to} \quad & \mathbf{x}_i^\top \Sigma_i \mathbf{x}_i - \tau_i \leq M z_i \quad \forall i \in [m], \\ & \mathbf{1}_{n_i}^\top \mathbf{x}_i \geq b_i \quad \forall i \in [m], \\ & \mathbf{1}_n^\top \mathbf{x} = 1, \mathbf{x} \geq 0, \end{aligned}$$

where $M > 0$ is a large scalar. The equivalent MPCC formulation is given as

$$\begin{aligned} \min_{\mathbf{x}, \boldsymbol{\eta}, \boldsymbol{\xi}} \quad & -\mathbf{a}^\top \mathbf{x} + \lambda \mathbf{1}^\top (\mathbf{1} - \boldsymbol{\xi}) \\ \text{subject to} \quad & \eta_i \geq \mathbf{x}_i^\top \Sigma_i \mathbf{x}_i - \tau_i \quad \forall i \in [m], \\ & \mathbf{1}^\top \mathbf{x} = 1, \boldsymbol{\eta} \circ \boldsymbol{\xi} = 0, \mathbf{x} \geq 0, \\ & \mathbf{1}_{n_i}^\top \mathbf{x}_i \geq b_i, 0 \leq \xi_i \leq 1, \eta_i \geq 0 \quad \forall i \in [m]. \end{aligned}$$

In the MPCC-DC formulation, the complementarity constraint ($\boldsymbol{\eta} \circ \boldsymbol{\xi} = 0$) is removed from the above model, and the objective is updated as

$$\min_{\mathbf{x}, \boldsymbol{\eta}, \boldsymbol{\xi}} -\mathbf{a}^\top \mathbf{x} + \lambda \mathbf{1}^\top (\mathbf{1} - \boldsymbol{\xi}) + \gamma \sum_{i=1}^m \min\{\eta_i, \xi_i\}.$$

Finally, the Direct-DC formulation is given as

$$\begin{aligned} \min_{\mathbf{x}} -\mathbf{a}^\top \mathbf{x} + \lambda \sum_{i \in [m]} \left[\max \left\{ \frac{1}{\epsilon} (\mathbf{x}_i^\top \Sigma_i \mathbf{x}_i - \tau_i), 0 \right\} - \max \left\{ \frac{1}{\epsilon} (\mathbf{x}_i^\top \Sigma_i \mathbf{x}_i - \tau_i) - 1, 0 \right\} \right] \\ \text{subject to } \mathbf{1}^\top \mathbf{x} = 1, \mathbf{x} \geq 0, \mathbf{1}_{n_i}^\top \mathbf{x}_i \geq b_i \quad \forall i \in [m]. \end{aligned}$$

In our numerical experiment, we use $\lambda = 100$ in the MIP, MPCC, MPCC-DC, and Direct-DC formulations. Additionally, we set $M = 10^6$ in the MIP model, $\gamma = 110$ in MPCC-DC, and $\epsilon = 1500$ in Direct-DC. For each of the 13 sectors, we set the threshold of violation to the square root of the maximum diagonal element of the covariance matrix of the corresponding sector.

A.2 Intensity-modulated radiation therapy planning problem

For the IMRT problem in (18), we introduce two models to serve as a benchmark for our approach. The first model is prevalent in radiation therapy planning literature focusing only on radiation precision. In this model, we penalize deviation from the prescribed dosage for healthy organs and tumors. This model formulation is stated as:

$$\begin{aligned} \min_{\mathbf{x}, \mathbf{y}} \alpha \sum_{v \in \mathcal{T}} (x_v - \mu)^2 + (1 - \alpha) \sum_{v \in \mathcal{H}} (x_v - \tau)^2 \\ \text{subject to } x_v = \sum_{b \in \mathcal{B}} d_{vb} y_b \quad \forall v \in \mathcal{V}, \\ \underline{y} \leq y_b \leq \bar{y} \quad \forall b \in \mathcal{B}. \end{aligned}$$

The hyperparameter $\alpha \in [0, 1]$ used in the objective function allows us to control the emphasis between the tumor and healthy organs. We refer to the above as the ‘‘quadratic penalty’’ (QP) model.

The CMP model for IMRT planning in (18) minimizes the number of healthy voxels receiving excess dosage. Alternatively, we can minimize the extent of over-dosage (beyond the prescribed dosage) for healthy voxels. The following model formulation, the ‘‘One-sided Quadratic Penalty’’

(1-QP), utilizes such an objective. We state it as:

$$\begin{aligned}
& \min_{\mathbf{x}, \mathbf{y}, \mathbf{z}} \sum_{v \in \mathcal{T}} (x_v - \mu)^2 + \bar{\lambda} \sum_{v \in \mathcal{H}} z_v^2 \\
& \text{subject to: } x_v = \sum_{b \in \mathcal{B}} d_{vb} y_b \quad \forall v \in \mathcal{V}, \\
& \quad z_v \geq x_v - \tau \quad \forall v \in \mathcal{H}, \\
& \quad z_v \geq 0 \quad \forall v \in \mathcal{H}, \\
& \quad \underline{y} \leq y_b \leq \bar{y} \quad \forall b \in \mathcal{B}.
\end{aligned}$$

Like the CMP model (18), and unlike the QP model, the above program does not penalize any deviation from prescriptions for healthy voxels if the amount of radiation received by such voxels is less than the corresponding prescribed threshold. Note that the parameter $\bar{\lambda}$ plays a similar role as λ in the CMP.

For completion, we also present the approximate models. First, the model obtained by employing the MPCC-DC approach in §2.1 is given as

$$\begin{aligned}
& \min_{\mathbf{x}, \mathbf{y}, \boldsymbol{\eta}, \boldsymbol{\xi}} \sum_{v \in \mathcal{T}} (x_v - \mu)^2 + \sum_{v \in \mathcal{H}} (\lambda(1 - \xi_v) + \gamma \min\{\eta_v, \xi_v\}) \\
& \text{subject to } x_v = \sum_{b \in \mathcal{B}} d_{vb} y_b \quad \forall v \in \mathcal{V}, \\
& \quad \underline{y} \leq y_b \leq \bar{y} \quad \forall b \in \mathcal{B}, \\
& \quad \eta_v \geq x_v - \tau \quad \forall v \in \mathcal{H}, \\
& \quad 0 \leq \xi_v \leq 1, \eta_v \geq 0 \quad \forall v \in \mathcal{H}.
\end{aligned}$$

The formulation resulting from the Direct-DC approach, presented in §2.2, is as follows.

$$\begin{aligned}
& \min_{\mathbf{x}, \mathbf{y}} \sum_{v \in \mathcal{T}} (x_v - \mu)^2 + \tag{19} \\
& \quad \lambda \sum_{v \in \mathcal{H}} \left[\max \left\{ \frac{1}{\varepsilon} (x_v - \tau), 0 \right\} - \max \left\{ \frac{1}{\varepsilon} (x_v - \tau) - 1, 0 \right\} \right] \\
& \text{subject to } x_v = \sum_{b \in \mathcal{B}} d_{vb} y_b \quad \forall v \in \mathcal{V}, \\
& \quad \underline{y} \leq y_b \leq \bar{y} \quad \forall b \in \mathcal{B}.
\end{aligned}$$

As with the portfolio optimization problem, the IMRT problem (18) also admits a mixed-binary program as an equivalent formulation. Unfortunately, we could not obtain solutions from this formulation for any dataset using the default integer programming solvers in Gurobi. Therefore, we did not consider the mixed-binary programs in our numerical experiments.

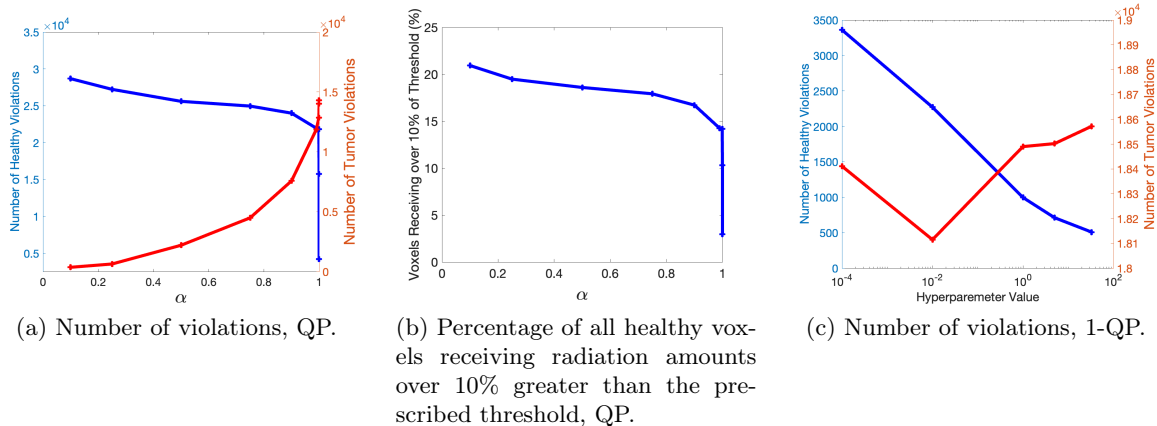


Figure 6: Number of violations for healthy voxels and for tumorous voxels as hyperparameter value changes for the QP method for Dataset 1.

A.3 Benchmark methods and hyperparameters

In this section, we discuss hyperparameter selection for the benchmark models for the IMRT problem detailed in section A.2. First, the QP method experiences a clear trade-off between adherence to healthy voxels' prescriptions and tumorous voxels' prescriptions as hyperparameter values change (see Figure 6a). We see more healthy voxel violations with hyperparameter values near 1 even though these hyperparameter values indicate more emphasis on the objective term relating to healthy voxels. This counterintuitive nature is attributed to the relative increase in average violation magnitude; for hyperparameter values near 1, each violation magnitude is relatively small. Conversely, for hyperparameter values near 0, the quadratic nature of the penalty decays and instead "sacrifices" some voxels so that large quantities of other voxels may meet requirements. We also note that the QP method tends to result in large quantities of healthy voxels receiving radiation levels over 10% greater than the prescribed threshold (see Figure 6b). Any IMRT treatment with this quality is unacceptable. Therefore, in §3.3 we use $\alpha = 1 - 10^{-6}$ as this value typically results in approximately 3% – 5% of total healthy voxels receiving over 10% of the prescribed threshold. While this 3% – 5% value is chosen arbitrarily, it nevertheless provides a more practical solution to use in a real IMRT settings.

Next, the 1-QP method also experiences a trade-off as hyperparameter values change. However, this method results in less extreme exposure to radiation of healthy voxels as compared to the QP method. Also, the trade-off is less counterintuitive than in the QP method. Here, as less weight is placed on the terms relating to healthy voxels, fewer tumorous voxels receive insufficient radiation, and more healthy voxels receive excess radiation. Figure 6c details how the adherence to these two objectives changes as hyperparameter values change. We note that $\bar{\lambda} = .01$ results in similar radiation dosage patterns for tumorous voxels to the DC method results. Therefore, we choose this hyperparameter value for comparisons enumerated in §3.3.

References

- [1] M. Ahn, J.S. Pang, and J. Xin. Difference-of-convex learning: directional stationarity, optimality, and sparsity. *SIAM Journal on Optimization*, 27(3):1637–1665, January 2017.
- [2] A. Al-Shabili, Y. Feng, and I. Selesnick. Sharpening sparse regularizers via smoothing. *IEEE Open Journal of Signal Processing*, 2:396–409, 2021.
- [3] Edoardo Amaldi, Marc E Pfetsch, and Leslie E Trotter, Jr. On the maximum feasible subsystem problem, iiss and iis-hypergraphs. *Mathematical Programming*, 95:533–554, 2003.
- [4] K. Bui, F. Park, S. Zhang, Y. Qi, and J. Xin. Structured sparsity of convolutional neural networks via nonconvex sparse group regularization. *Frontiers in Applied Mathematics and Statistics*, 6, February 2021.
- [5] E. Candés, M. Wakin, and S. Boyd. Enhancing sparsity by reweighted ℓ_1 minimization. *Journal of Fourier Analysis and Applications*, 14(5-6):877–905, 2008.
- [6] M. Ehrgott, C. Guler, H. Hamacher, and L. Shao. Mathematical optimization in intensity modulated radiation therapy. *Annals of Operations Research*, 175(1):309–365, 2010.
- [7] F. Facchinei and J.S. Pang, editors. *Finite-Dimensional Variational Inequalities and Complementarity Problems*. Springer New York, 2004.
- [8] J. Fan and J. Lv. A selective overview of variable selection in high dimensional feature space. *Statistica Sinica*, 20(1):101–148, 2010.
- [9] M. Feng, J.E. Mitchell, J.S. Pang, A. Waechter, and X. Shen. Complementarity formulations of ℓ_0 -norm optimization problems. *Pacific Journal of Optimization*, 14(2):273–305, 2018.
- [10] Kenneth French. Data library. Online.
- [11] Archis Ghate. *Optimal Fractionation in Radiotherapy*. Cambridge University Press, 2023.
- [12] M. Ho, Z. Sun, and J. Xin. Weighted elastic net penalized mean-variance portfolio design and computation. *SIAM Journal on Financial Mathematics*, 6(1):1220–1244, 2015.
- [13] D. Jaffray. Image-guided radiotherapy: from current concept to future perspectives. *Nature Reviews Clinical Oncology*, 9(12):688–699, 2012.
- [14] F. Jara-Moroni, J.S. Pang, and A. Wächter. A study of the difference-of-convex approach for solving linear programs with complementarity constraints. *Mathematical Programming*, 169(1):221–254, 2018.
- [15] H.A. Le Thi and T. Pham Dinh. On solving linear complementarity problems by DC programming and DCA. *Computational Optimization and Applications*, 50(3):507–524, 2011.

- [16] H.A. Le Thi, T. Pham Dinh, H.M. Le, and X.T. Vo. DC approximation approaches for sparse optimization. *European Journal of Operational Research*, 244(1):26–46, 2015.
- [17] W. Li, W. Bian, and K-C Toh. Difference-of-convex algorithms for a class of sparse group ℓ_0 regularized optimization problems. *SIAM Journal on Optimization*, 32(3):1614–1641, 2022.
- [18] M. Nikolova. Local strong homogeneity of a regularized estimator. *SIAM Journal on Applied Mathematics*, 61(2):633–658, 2000.
- [19] M. Norton, A. Mafusalov, and S. Uryasev. Cardinality of upper average and its application to network optimization. *SIAM Journal on Optimization*, 28(2):1726–1750, January 2018.
- [20] J.S. Pang, M. Razaviyayn, and A. Alvarado. Computing b-stationary points of nonsmooth DC programs. *Mathematics of Operations Research*, 42(1):95–118, January 2017.
- [21] F. Saberian, A. Ghatte, and M. Kim. Spatiotemporally optimal fractionation in radiotherapy. *INFORMS Journal on Computing*, 29(3):422–437, 2017.
- [22] B. Sriperumbudur and G. Lanckriet. A proof of convergence of the concave-convex procedure using Zangwill’s theory. *Neural Computation*, 24(6):1391–1407, 06 2012.
- [23] Andreas M Tillmann, Daniel Bienstock, Andrea Lodi, and Alexandra Schwartz. Cardinality minimization, constraints, and regularization: a survey. *arXiv preprint arXiv:2106.09606*, 2021.
- [24] D. Troxell, M. Ahn, and H. Gangammanavar. A cardinality minimization approach for security-constrained economic dispatch. *IEEE Transactions on Power Systems*, 37(5):3642–3652, 2021.
- [25] C. Wang, M. Tao, J. Nagy, and Y. Lou. Limited-angle CT reconstruction via the L_1/L_2 minimization. *SIAM Journal on Imaging Sciences*, 14(2):749–777, 2021.